Optimized Susceptibility MRI Sequences for Novel Diagnostic Biomarkers of Multiple Sclerosis

Sreekanth Madhusoodhanan Nair[1], Jin Jin[2], Chang Gao[3], Nader Binesh[4], Thomas Benkert[5], Marcel Maya[4], Pascal Sati[1]

[1] Neuroimaging Program, Department of Neurology, Cedars-Sinai Medical Center, Los Angeles, CA, USA
[2] Siemens Healthineers Pty Ltd, Brisbane, Australia
[3] Siemens Healthineers, Los Angeles, USA
[4] Department of Imaging, Cedars-Sinai Medical Center, Los Angeles, CA, USA
[5] Siemens Healthineers, Erlangen, Germany

Introduction

The 2024 revisions of the international diagnostic criteria for multiple sclerosis (MS) [1] provide an expanded role for magnetic resonance imaging (MRI) by incorporating two novel imaging biomarkers: the central vein sign (CVS) [2] and paramagnetic rim lesions (PRL) [3]. Recent MRI guidelines by the MAGNIMS-CMSC-NAIMS consortia provide practical guidance for the implementation of the different MRI sequences required for the accurate biomarker detection and precise identification of MS [4]. In this article, we focus specifically on the implementation of the susceptibility MRI sequences required for the detection of CVS and PRL.

Due to their paramagnetic properties, CVS and PRL can be detected non-invasively using susceptibility MRI sequences. More specifically, susceptibility-weighted imaging (SWI) has emerged as an important additional sequence to the diagnostic brain MRI protocol for MS since it is highly sensitive to venous features and iron-related signals in the white matter lesions that would be otherwise invisible on conventional T1- and T2-weighted sequences [5, 6]. Although standard SWI provides filtered phase images that are adequate for PRL detection, the SWI magnitude images are not optimized for standalone CVS detection. This complicates the diagnostic interpretation workflow for practitioners. Additionally, standard SWI relies on a gradient echo (GRE) acquisition, which cannot provide in a clinically feasible scan time the recommended submillimeter isotropic resolution for the highest confidence in CVS and PRL detection [4]. An alternative strategy for overcoming this issue for CVS detection is the use of T2*-weighted 3D-segmented echo-planar imaging (3D EPI) [7].

In this article, we will review these techniques and provide guidance for the clinical implementation of an optimized SWI-GRE protocol[1] for concomitant evaluation of CVS and PRL, and of a submillimeter T2* 3D EPI protocol for reaching highest detection confidence for CVS and PRL.

MRI acquisitions

All the cases presented here were imaged on 3T MRI scanners (MAGNETOM Skyra and MAGNETOM Vida) using 20-channel head/neck coils at Cedars-Sinai Medical Center (Los Angeles, CA, USA). Two different brain SWI protocols using the same spatial resolution and coverage were implemented: (a) standard SWI-GRE with a flip angle (FA) of 15°, and (b) optimized SWI-GRE with an FA of 5°. All other sequence parameters were the same in both the standard and optimized SWI-GRE protocols. Additionally, the 3D EPI sequence ('ep_seg_fid'), available in the default sequence tree from Siemens Healthineers (Fig. 1) for recent software versions (≥ VA31), was used to implement submillimeter isotropic T2*-weighted acquisition. Details of the sequence parameters used are shown in Table 1.

[1] *3D EPI SWI processing is provided via a research application[x] resulting in filtered phase images as well as SWI magnitude images.*
[x] *Work in progress. The application is currently under development and is not for sale in the U.S. and in other countries. Its future availability cannot be ensured.*

Protocol	Optimized SWI-GRE	T2* 3D EPI
TE (ms)	20	35
TR (ms)	27	65
FA (deg)	5	10
In-plane resolution (mm²)	0.7 × 0.7	0.7 × 0.7
Slice thickness (mm)	2	0.7
FOV Read (mm)	250	250
FOV Phase (%)	81.3	81.3
Base resolution	384	384
Acceleration factor	GRAPPA (2)	None
EPI factor	None	15
Bandwidth (Hz/px)	120	394
Reconstruction	Magn/Phase	Magn/Phase
Coil combination	Adaptive Combine	Adaptive Combine
Scan time	3:50 minutes	5:08 minutes

Table 1: MRI acquisition parameters for optimized SWI and T2* 3D EPI at 3-tesla.

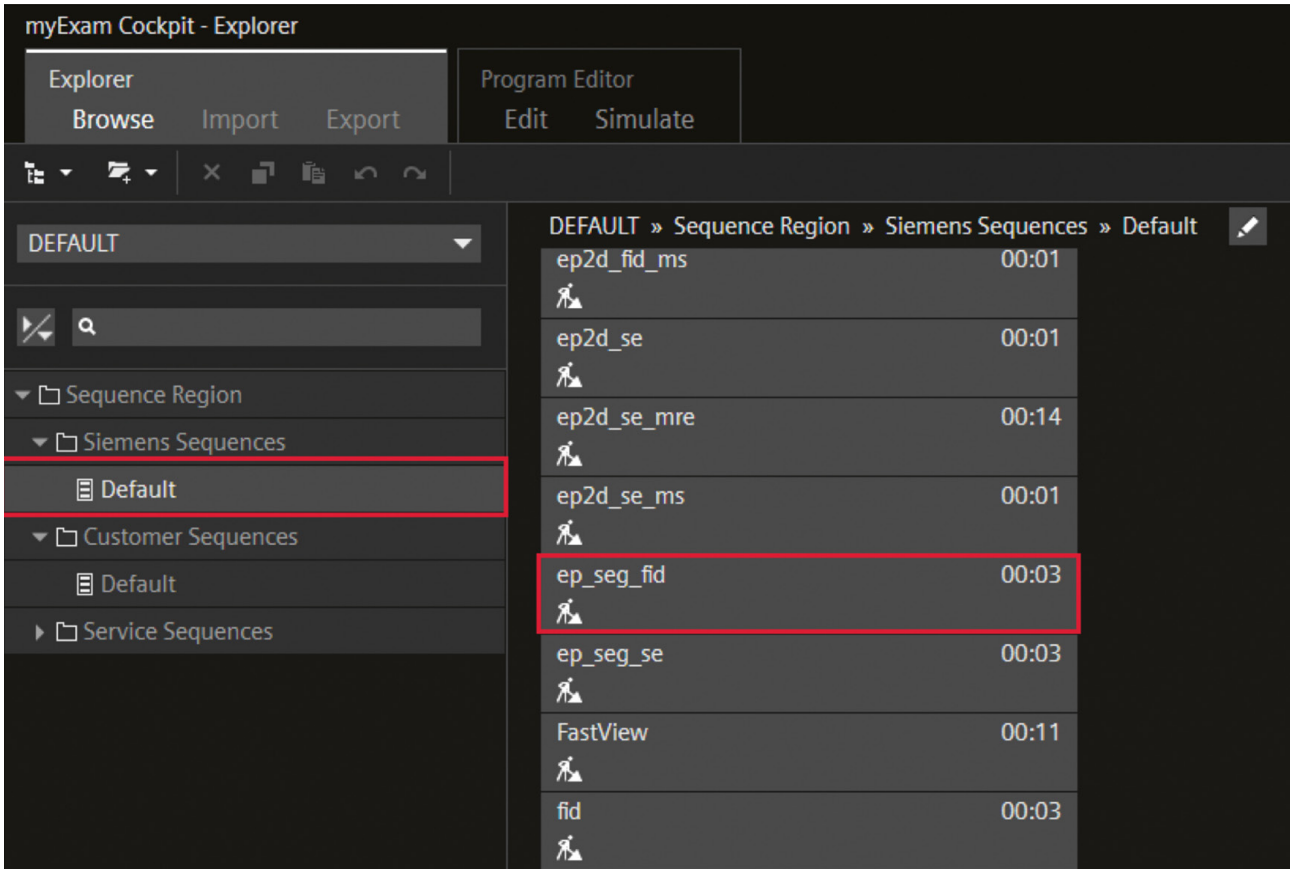

1 Product 3D EPI sequence ('ep_seg_fid') as it appears in the default sequence tree from Siemens Healthineers.

SWI-GRE

As a reminder, the standard SWI-GRE protocol was initially designed for assessing cerebral vasculature and hemorrhage [8, 9]. SWI is particularly useful for evaluating patients with stroke, vascular malformations, and venous diseases [6, 8], but it is not optimized for evaluating the CVS in patients with MS. Indeed, the standard SWI-GRE acquisition prioritizes maximal signal intensity with an FA near to the Ernst angle (between 15° and 20°), which introduces substantial T1-weighted contrast when repetition time (TR) is short. This T1 weighting significantly reduces the lesion-to-white-matter contrast and prevents the co-localization of MS lesions and central veins on SWI magnitude images. This issue is illustrated in Figure 2, where MS lesions appear largely isointense or hypointense on SWI magnitude images, thus requiring the use of T2 FLAIR images to co-localize the presence of T2 hyperintense lesions. In addition, the evaluation of CVS requires establishing the vein centrality using a precise co-registration between T2 FLAIR and SWI. This further complicates the interpretation workflow in clinical practice and reduces the reliability of the CVS rating if the T2 FLAIR and SWI images are inadequately aligned. On the other hand, SWI filtered phase images can be used for PRL evaluation and should be preferred over SWI magnitude images due to their higher sensitivity for PRL detection [10]. In Figure 2, a hypointense rim with isointense core depicting chronic active inflammation in the lesion is clearly visible in the filtered phase image. Note that the image intensity of the filtered phase images is displayed in the left-handed system by default on scanners from Siemens Healthineers. Therefore, the intensity of the filtered phase images needs to be inverted to match the right-handed convention recommended for the detection of PRL (e.g., paramagnetic rims and blood vessels appear dark) [3].

Optimized SWI-GRE

One way to improve diagnostic accuracy and workflow with SWI-GRE is to optimize the acquisition protocol for adequate detection of lesions and central veins on magnitude images. A simple protocol modification is to lower the FA (from 15° to 5° at 3T) to reduce T1 weighting and increase lesion visibility [11]. This single change in the sequence parameter does not affect the scan duration and enables the standalone detection of CVS. This is shown in

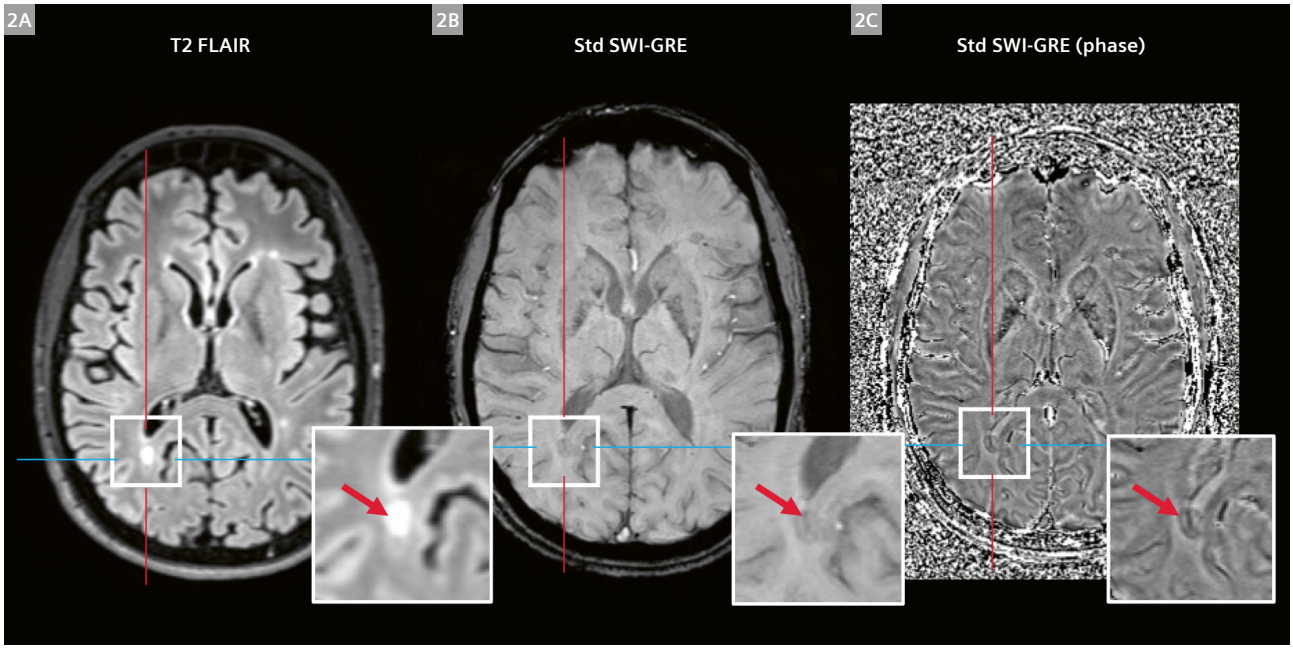

2 **(2A)** Focal hyperintense lesions on T2 FLAIR images, **(2B)** corresponding susceptibility-weighted (SWI) enhanced magnitude image and **(2C)** filtered phase image. Lesions appear isointense on the SWI enhanced magnitude image. For detection of the central vein sign (CVS), centrality of the vein needs to be confirmed using the crosshair. Paramagnetic rim lesion (PRL) is more clearly visible on the filtered phase image than the enhanced magnitude image.

Figure 3, which compares the two SWI protocols (standard and optimized[1]) acquired in the subjects with MS. Hyperintense focal white matter lesions identified on T2 FLAIR are invisible on standard SWI magnitude images but appear hyperintense on the optimized SWI magnitude images (red arrows). As a result, the presence of a central hypointense vein inside these focal white matter lesions can be demonstrated easily with the optimized SWI magnitude images. An important additional observation is that the change in FA does not impact the detection of incidental microbleed (blue arrows). Moreover, the detection of PRL is not affected by the change in FA, as shown in Figure 3, where both SWI filtered phase images display similar detection sensitivity (white arrows). Additional examples illustrating the superior detection of CVS-positive lesions achieved with the optimized SWI are shown in Figure 4 (top two rows). Examples of the superior detection of PRL-positive lesions achieved with SWI filtered phase images over SWI magnitude images are also shown in Figure 4 (bottom two rows).

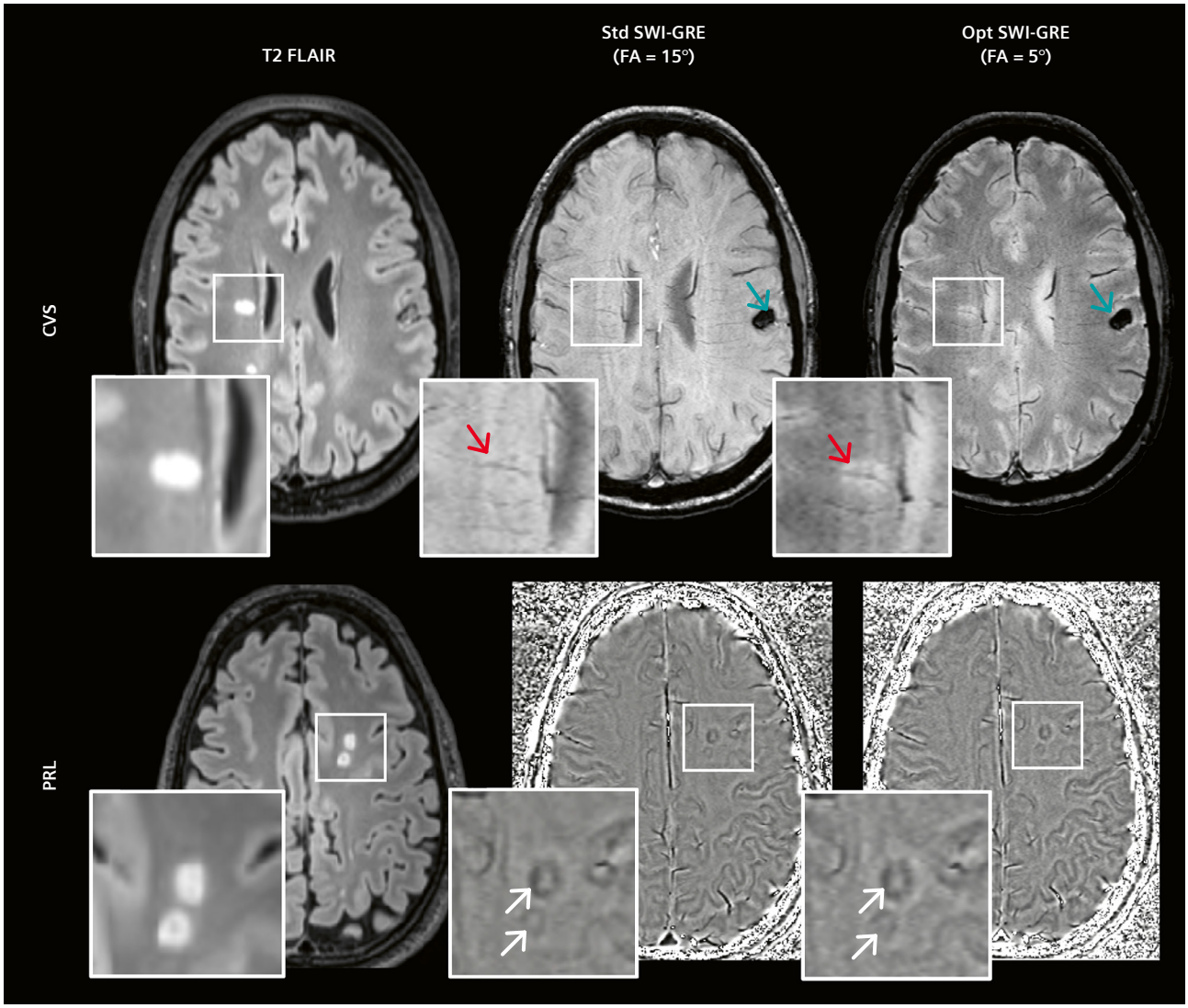

3 Head-to-head comparison of standard and optimized SWI-GRE images acquired in the same subjects with multiple sclerosis. T2 FLAIR images show focal hyperintense lesions in the periventricular and deep white matter areas. Standard SWI-GRE (FA = 15°) shows limited lesion conspicuity with isointense contrast, whereas optimized SWI-GRE (FA = 5°) clearly depicts CVS with high tissue contrast (hyperintense lesion with hypointense vein) (red arrow). A hemorrhagic bleed shows comparable sensitivity on both SWI acquisitions (blue arrow). Bottom panels: On filtered phase images, PRL demonstrates equal sensitivity with both SWI protocols (white arrows).

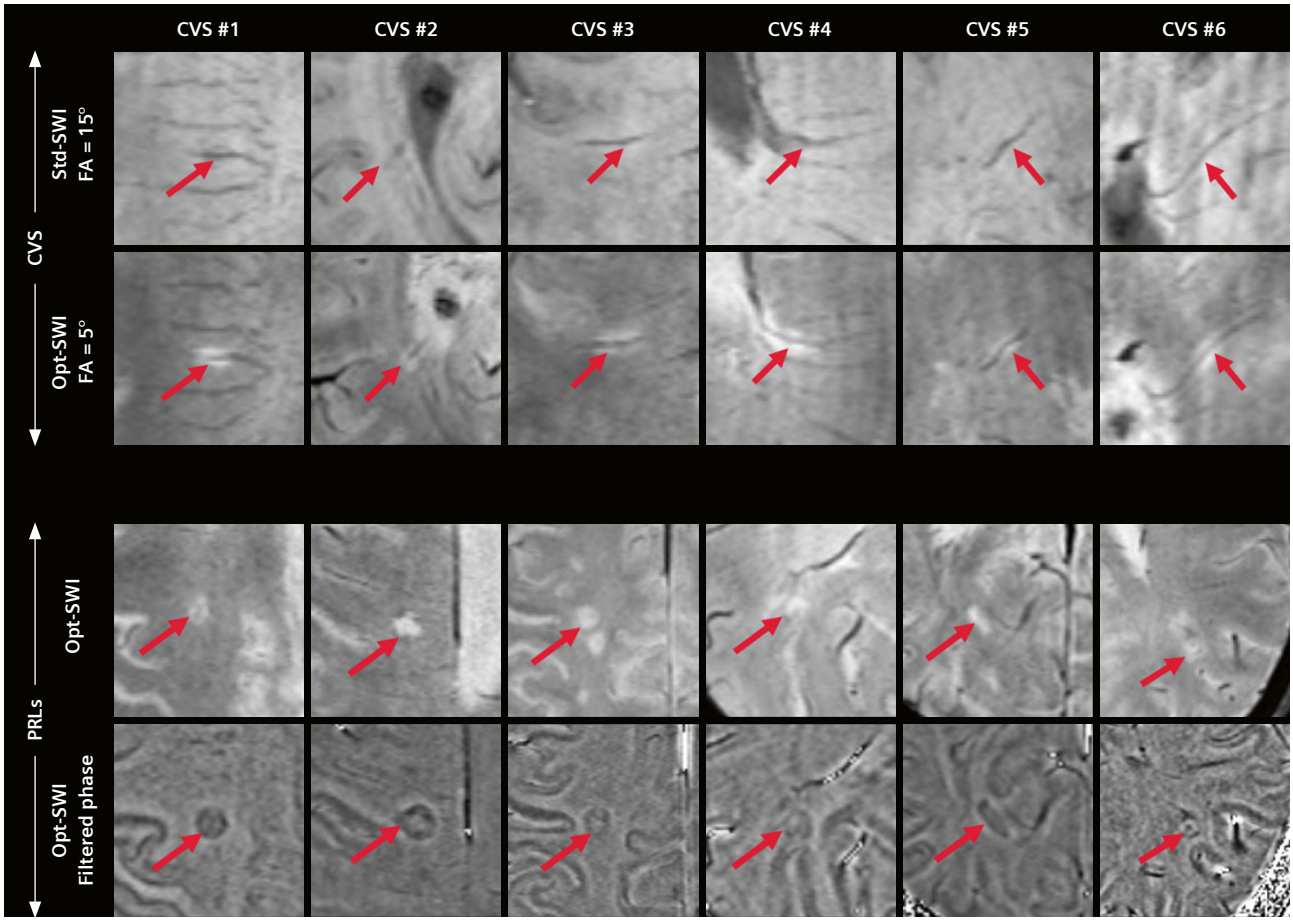

4 The top two rows demonstrate the standalone CVS detection sensitivity of SWI-GRE acquisition at two flip angles, illustrated in the same MS patient evaluated for Select6 criteria (6 or more CVS positive lesions as per the 2024 revised MS diagnostic criteria). The bottom two rows exhibit the superior PRL detection sensitivity, illustrated in six patients with MS. A hypointense rim with an isointense core indicating chronic active inflammation is clearly visible in the filtered phase images, unlike in the SWI magnitude images.

T2*-weighted 3D EPI

The international MRI guidelines recently published by the MAGNIMS-CMSC-NAIMS consortia recommend using submillimeter isotropic T2*-weighted and filtered phase images for more sensitive and reliable detection of the CVS and PRL [2–4]. The product version of the 3D EPI sequence [7, 12] (available for software versions ≥ *syngo* MR VA31) enables the acquisition of magnitude and phase images at 0.65–0.8 mm isotropic in a clinically feasible scan time of 4–6 minutes without the use of parallel imaging acceleration (Table 1). SWI processing is provided via a research application[×], resulting in filtered phase images as well as SWI magnitude images. Representative examples from an MS subject scanned with the 3D EPI protocol are shown in Figure 5. The CVS is clearly visible in all three planes of the T2*-weighted 3D EPI images (red arrows). Similarly, PRL is clearly visible in all three planes of the filtered phase images from 3D EPI (white arrows). This multi-planar evaluation increases reader confidence in rating the CVS and PRL, and reduces any potential false-positive detection. Note the difference in image quality when reformatting the SWI images in coronal and sagittal views. This is due to the anisotropic voxel dimensions which hinders the multi-planar assessment of CVS and PRL (Fig. 5, bottom two rows).

[×] *Work in progress. The application is currently under development and is not for sale in the U.S. and in other countries. Its future availability cannot be ensured.*

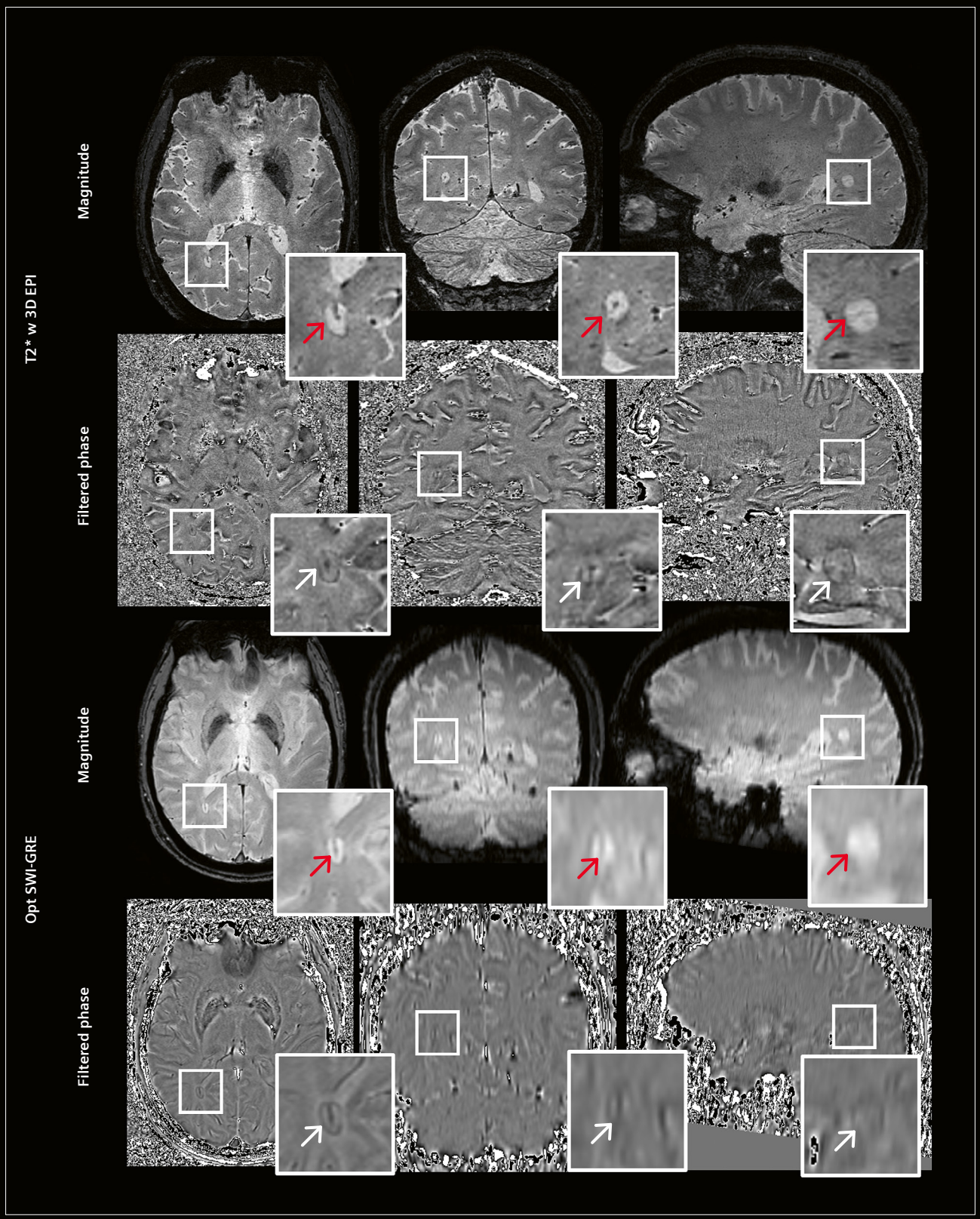

5 Multiplanar view of optimized T2*-weighted 3D EPI (top) and SWI-GRE (bottom) acquired on the same MS patient. High-resolution isotropic acquisition in T2*-weighted 3D EPI enables clear visualization of CVS and PRL in all imaging planes.

Discussion and conclusions

Given the need for rapid clinical adoption of the new imaging biomarkers recently included in the revised diagnostic criteria for MS, we provide here practical strategies to integrate adequate susceptibility MRI sequences into the diagnostic imaging workflow. We recommend using an optimized SWI protocol at 3-tesla to ensure sensitive detection of CVS, and filtered phase images for sensitive detection of PRL. When possible, the more advanced 3D EPI sequence is recommended to acquire submillimeter isotropic images. This enables multi-planar evaluation of T2*-weighted and filtered phase images and increases the radiologist's confidence in interpreting CVS and PRL. Our recommended MRI protocols for these sequences are available for download (see QR code) or can be requested directly via local Siemens support. Finally, work is currently underway on technical developments that are using advanced acceleration strategies and deep-learning reconstruction methods to further reduce acquisition time and facilitate wider implementation of these sequences in the clinical setting.

Contact

Sreekanth Madhusoodhanan Nair, Ph.D.
Postdoctoral Scientist
Neuroimaging Program
Department of Neurology
Cedars-Sinai Medical Center
Atrium Building, 2nd Floor
8750 Beverly Blvd
Los Angeles, CA 90048
USA
Sreekanth.madhusoodhanan@cshs.org

Pascal Sati, Ph.D.
Associate Professor
Director of Neuroimaging Program
Department of Neurology
Cedars-Sinai Medical Center
Atrium Building, 2nd Floor
8750 Beverly Blvd
Los Angeles, CA 90048
USA
Pascal.sati@cshs.org

Marcel Maya, M.D.
Professor and Co-Chair
Department of Imaging
Cedars-Sinai Medical Center
8700 Beverly Blvd, Room M335
Los Angeles, CA 90048
USA
Marcel.maya@cshs.org

Acknowledgments

We acknowledge the support of the National Institute of Neurological Disorders and Stroke (NINDS), the National Multiple Sclerosis Society (NMSS), the Department of Defense (DoD), and the Erwin Rautenberg Foundation.

Appendix

Download the optimized SWI and T2* EPI protocol for different scanner models from:

magnetomworld.siemens-healthineers.com/clinical-corner/protocols/neurology-neurography/mri-sequences

References

1 Montalban X, Lebrun-Frénay C, Oh J, Arrambide G, Moccia M, Amato MP, et al. Diagnosis of multiple sclerosis: 2024 revisions of the McDonald criteria. Lancet Neur. 2025;24(10):850–865.
2 Sati P, Oh J, Constable RT, Evangelou N, Guttmann CR, Henry RG, et al. The central vein sign and its clinical evaluation for the diagnosis of multiple sclerosis: a consensus statement from the North American Imaging in Multiple Sclerosis Cooperative. Nat Rev Neurol. 2016;12(12):714–722.
3 Bagnato F, Sati P, Hemond CC, Elliott C, Gauthier SA, Harrison DM, et al. Imaging chronic active lesions in multiple sclerosis: a consensus statement. Brain. 2024;147(9):2913–2933.
4 Barkhof F, Reich DS, Oh J, Rocca MA, Li DK, Sati P, et al. 2024 MAGNIMS-CMSC-NAIMS consensus recommendations on the use of MRI for the diagnosis of multiple sclerosis. Lancet Neurol. 2025;24(10):866–879.
5 Clarke M, Pareto D, Pessini-Ferreira L, Arrambide G, Alberich M, Crescenzo F, et al. Value of 3T susceptibility-weighted imaging in the diagnosis of multiple sclerosis. AJNR Am J Neuroradiol. 2020; 41(6):1001–1008.
6 Mittal S, Wu Z, Neelavalli J, Haacke EM. Susceptibility-weighted imaging: technical aspects and clinical applications, part 2. AJNR Am J Neuroradiol. 2009;30(2):232–52.
7 Sati P, Patil S, Inati S, Wang W-T, Derbyshire JA, Krueger G, et al. Rapid MR susceptibility imaging of the brain using segmented 3D echo-planar imaging (3D EPI) and its clinical applications. ↗ MAGNETOM Flash. 2017;68(2):26–32.
8 Haacke EM, Xu Y, Cheng YCN, Reichenbach JR. Susceptibility weighted imaging (SWI). Magn Reson Med. 2004;52(3):612–8.
9 Haacke EM, Mittal S, Wu Z, Neelavalli J, Cheng Y-C. Susceptibility-weighted imaging: technical aspects and clinical applications, part 1. AJNR Am J Neuroradiol. 2009;30(1):19–30.
10 Lee JD, Renner B, Madhusoodhanan Nair S, Nakamura K, Luskin E, Shinohara RT, et al. Superior visibility of paramagnetic rim lesions on filtered phase versus SWI. AJNR Am J Neuroradiol. 2026:ajnr. A9295.
11 Madhusoodhanan Nair S, Hsu YC, Luskin E, Ayrapetyan D, Liu A, Binesh N, et al. Optimized Susceptibility Weighted Imaging for the Detection of Central Vein Sign in Multiple Sclerosis at 3-tesla. In: Proceedings of the Annual Meeting of ISMRM & ISMRT, Honolulu, Hawai'i, USA. 2025 May 10–15. ISMRM; 2025:3766.
12 Sati P, Thomasson DM, Li N, Pham DL, Biassou NM, Reich DS, et al. Rapid, high-resolution, whole-brain, susceptibility-based MRI of multiple sclerosis. Mult Scler. 2014;20(11):1464–70.